Research Article | Vol. 25, No. 4 | 20 Feb 2017 | OPTICS EXPRESS A73

Optics EXPRESS

IAOOS microlidar-on-buoy development and first atmospheric observations obtained during 2014 and 2015 arctic drifts

VINCENT MARIAGE,[1,2,*] JACQUES PELON,[1] FRÉDÉRIC BLOUZON,[3] STÉPHANE VICTORI,[2] NICOLAS GEYSKENS,[3] NADIR AMAROUCHE,[3] CHRISTINE DREZEN,[4] ANTOINE GUILLOT,[4] MICHEL CALZAS,[4] MAGALI GARRACIO,[5] NICOLAS WEGMULLER,[6] NATHALIE SENNÉCHAEL,[7] AND CHRISTINE PROVOST[7]

[1]*LATMOS/IPSL, UPMC Univ. Paris 06 Sorbonne Universités, UVSQ, CNRS, Paris, France*
[2]*Cimel Electronique, Paris, France*
[3]*DT/INSU, Meudon, France*
[4]*DT/INSU, Brest, France*
[5]*IPEV, Brest, France*
[6]*PIT, OVSQ, Guyancourt, France*
[7]*Laboratoire LOCEAN-IPSL, Sorbonne Universités (UPMC, Univ. Paris 6)-CNRS-IRD-MNHN, Paris, France*
[*]*vincent.mariage@latmos.ipsl.fr*

Abstract: The *in situ* tests of first ever autonomous aerosol and cloud backscatter LIDAR (light detection and ranging) systems implemented on buoys for Arctic observations has been achieved in 2015 within the French EQUIPEX IAOOS project. The environmental and operational constraints were met by adopting a concept of a fibered microjoule lidar system using a laser diode. Two systems have been developed with and without polarization analysis capability. A specific optical design was used for polarization discrimination. These systems were integrated in buoys and tested in the Arctic in 2014 and 2015 at latitudes higher than 80°N. Data were transmitted through an Iridium space link. Measurements have been obtained 90% of the time from the non-polarized system in 2014 over 8 months as the first fully equipped buoy drifted from the Barneo Russian camp close to the North Pole toward Svalbard. A polarized system was then tested over a short period in winter 2015 north of Svalbard during the Norwegian campaign N-ICE. In April and May 2014, the unattended lidar measurements showed a large occurrence of aerosols and haze. The average attenuated scattering ratio for non-cloudy profiles during this period was about 2.2. Aerosols could reach an altitude of 5km on average, whereas over the rest of the period low level clouds (below 1000 m) were prevailing with an average attenuated scattering ratio of about 10^3. The main features of the developed lidar instruments and first results are presented here

OCIS codes: (010.0010) Atmospheric and oceanic optics; (010.0280) Remote sensing and sensors; (010.3640) Lidar; (010.1350) Backscattering; (010.1615) Clouds.

References and links

1. M. D. Shupe and J. M. Intrieri, "Cloud radiative forcing of the arctic surface: the influence of cloud properties, surface albedo, and solar zenith angle," J. Clim. **17**(3), 616–628 (2004).
2. J. M. Intrieri, M. D. Shupe, T. Uttal, and B. J. McCarty, "An annual cycle of arctic cloud characteristics observed by radar and lidar at SHEBA," J. Geophys. Res. **107**, (C10), SHE 5–1–SHE 5–15 (2002).
3. J. M. Intrieri, C. W. Fairall, M. D. Shupe, P. O. G. Persson, E. L. Andreas, P. S. Guest, and R. E. Moritz, "An annual cycle of arctic surface cloud forcing at SHEBA," J. Geophys. Res. **107**, (C10), SHE 13–1–SHE 13–14 (2002).
4. D. M. Winker, J. Pelon, J. A. Coakley, Jr., S. A. Ackerman, R. J. Charlson, P. R. Colarco, P. Flamant, Q. Fu, R. Hoff, C. Kittaka, T. L. Kubar, H. LeTreut, M. P. McCormick, G. Megie, L. Poole, K. Powell, C. Trepte, M. A. Vaughan, and B. A. Wielicki, "The CALIPSO mission: a global 3D view of aerosols and clouds," Bull. Am. Meteorol. Soc. **91**(9), 1211–1229 (2010).

#279151 http://dx.doi.org/10.1364/OE.25.000A73
Journal © 2017 Received 3 Nov 2016; revised 24 Nov 2016; accepted 24 Nov 2016; published 13 Jan 2017

Optics EXPRESS

5. Y. Blanchard, J. Pelon, E. W. Eloranta, K. P. Moran, J. Delanoë, and G. Sèze, "A synergistic analysis of cloud cover and vertical distribution from A-Train and ground-based sensors over the high arctic station Eureka from 2006 to 2010," J. Appl. Meteorol. Climatol. **53**(11), 2553–2570 (2014).
6. S. Tanelli, S. L. Durden, E. Im, K. S. Pak, D. G. Reinke, P. Partain, J. M. Haynes, and R. T. Marchand, "CloudSat's cloud profiling radar after two years in orbit: performance, calibration and processing," IEEE Trans. Geosci. Remote Sens. **46**(11), 3560–3573 (2008).
7. C. Provost, J. Pelon, N. Sennéchael, M. Calzas, F. Blouzon, A. Desautez, J. Descloitres, J.-C. Gascard, N. Villacieros-Robineau, V. Mariage, J.-P. Pommereau, T. Foujol, C. Drezen, A. Guillot, N. Geyskens, N. Amarouche, A. Sarkissian, N. Pascal, M. Garracio, P. D. Mahé, J. Sayadi, J. J. Correia, P. Genau, N. Wegmüller, and J. L. Maria, "IAOOS (Ice-Atmosphere-Arctic Ocean Observing System, 2011-2019)," Mercator Ocean Quarterly Newsletter **51**, 13–15 (2015).
8. K. M. Markowicz, P. J. Flatau, A. E. Kardas, J. Remiszewska, K. Stelmaszczyk, and L. Wöste, "Ceilometer retrieval of the boundary layer vertical aerosol extinction structure," J. Atmos. Ocean. Technol. **25**(6), 928–944 (2008).
9. S. Emeis, K. Schäfer, C. Münkel, R. Friedl, and P. Suppan, "K. Schäfer C. Münkel, R. Friedl, and P. Suppan, "Evaluation of the interpretation of ceilometer data with RASS and radiosonde data," Boundary-Layer Meteorol. **143**(1), 25–35 (2012).
10. M. Wiegner, F. Madonna, I. Binietoglou, R. Forkel, J. Gasteiger, A. Geiß, G. Pappalardo, K. Schäfer, and W. Thomas, "What is the benefit of ceilometers for aerosol remote sensing? an answer from EARLINET," Atmos. Meas. Tech. **7**(7), 1979–1997 (2014).
11. M. Wiegner and A. Geiß, "Aerosol profiling with the Jenoptik ceilometer CHM15kx," Atmos. Meas. Tech. **5**(8), 1953–1964 (2012).
12. J. R. Campbell, D. L. Hlavka, E. J. Welton, C. J. Flynn, D. D. Turner, J. D. Spinhirne, V. S. Scott III, and I. H. Hwang, "Full-time, eye-safe cloud and aerosol lidar observation at atmospheric radiation measurement program sites: instrument and data processing," J. Atmos. Ocean. Technol. **19**(4), 431–442 (2002).
13. M. L. Larsen and A. B. Kostinski, "Simple dead-time corrections for discrete time series of non-Poisson data," Meas. Sci. Technol. **20**(9), 095101 (2009).
14. G. P. Anderson, S. A. Clough, F. X. Kneizys, J. H. Chetwynd, and E. P. Shettle, "AFGL atmospheric constituent profiles (0-120km)," Air Force Geophysics Lab, Hanscom AFB, Maine Environmental Research Paper (1986).
15. E. J. O'Connor, A. J. Illingworth, and R. J. Hogan, "A technique for autocalibration of cloud lidar," J. Atmos. Ocean. Technol. **21**(5), 777–786 (2004).
16. C. M. R. Platt, "Lidar and radiometric observations of cirrus cloud," J. Atmos. Sci. **30**(6), 1191–1204 (1973).
17. R. G. Pinnick, S. G. Jennings, P. Chylek, C. Ham, and W. T. Grandy, Jr., "Backscatter and extinction in water clouds," J. Geophys. Res. **88**(C11), 6787–6796 (1983).
18. R. J. Hogan, "Fast approximate calculation of multiply scattered lidar returns," Appl. Opt. **45**(23), 5984–5992 (2006).
19. V. Freudenthaler, M. Esselborn, M. Wiegner, B. Heese, M. Tesche, A. Ansmann, D. Müller, D. Althausen, M. Wirth, A. Fix, G. Ehret, P. Knippertz, C. Toledano, J. Gasteiger, M. Garhammer, and M. Seefeldner, "Depolarization ratio profiling at several wavelengths in pure saharan dust during SAMUM 2006," Tellus B Chem. Phys. Meterol. **61**(1), 165–179 (2009).
20. B. Liu and Z. Wang, "Improved calibration method for depolarization lidar measurement," Opt. Express **21**(12), 14583–14590 (2013).
21. G. David, A. Miffre, B. Thomas, and P. Rairoux, "Sensitive and accurate dual-wavelength UV-VIS polarization detector for optical remote sensing of tropospheric aerosols," Appl. Phys. B **108**(1), 197–216 (2012).
22. C. Y. She, "Spectral structure of laser light scattering revisited: bandwidths of nonresonant scattering lidars," Appl. Opt. **40**(27), 4875–4884 (2001).
23. K. Sassen and R. L. Petrilla, "Lidar depolarization from multiple scattering in marine stratus clouds," Appl. Opt. **25**(9), 1450–1459 (1986).
24. K. Sassen, K. Kayetha, and J. Zhu, "Ice cloud depolarization for nadir and off-nadir CALIPSO measurements," Geophys. Res. Lett. **39**(20), L20805 (2012).

1. Introduction

The understanding of the arctic region changes is of main importance in particular because temperature changes due to global warming are larger there. The analysis of the still poorly-known ocean-ice-atmosphere interactions is required to have a better understanding of these changes. On the atmospheric side, the importance of measuring the vertical profiles of clouds properties (type, height and optical/microphysical properties) has been emphasized to allow a better understanding of interactions and a more accurate determination of the arctic cloud radiative forcing at the surface [1]. To access such information, vertically resolved measurements are needed, and it has been proposed in the frame of the french IAOOS (Ice-Atmosphere-Ocean-Observing System) EQUIPEX (EQUIPement d'EXcellence) project to focus on LIDAR measurements to perform new observations in the high arctic region (above 75°N). Only a few campaigns have previously been performed to analyze arctic cloudiness, over central Arctic especially when considering seasonal duration. Among them, the SHEBA

Optics EXPRESS

campaign (October 1997- October 1998), whose main goal was the estimation of heat budget in the Arctic, was the first to involve lidar measurements and provided very valuable quantitative data (cloud occurrence, type and properties) and analysis (cloud radiative forcing) between 75 and 78°N [2,3]. Regular observations are now conducted from a few land stations north of 70°N in the frame of the International Arctic Systems for Observing the Atmosphere (IASOA, http://www.esrl.noaa.gov/psd/iasoa/home2). All stations include active sensors to derive cloud information, but they are all located below 82°N. Satellite observations provide the necessary regional and temporal coverage, but visible radiometry offers reduced performance over arctic due to bright surface contamination. As part of new sensors less affected by this problem, the Cloud and Aerosol Lidar and Infrared Pathfinder Space Observation (CALIPSO) space mission is giving access to the vertical cloud distribution using lidar measurements [4]. Still, the lower layers of the atmosphere may be occulted by upper dense layers [5]. Radar observations from the Cloud Satellite (CloudSat) mission are also perturbed in this region by surface clutter and lack sensitivity for water clouds [6], which occurrence is critical [1]. Both satellite missions do not allow the very high arctic regions above 82°N to be sampled.

The main goal of the IAOOS project is to bridge this gap by deploying a network of autonomous drifting buoys deployed over the high central arctic region. These buoys have been designed to embark a lidar system, meteorological sensors, snow and ice temperature profiler and ocean profilers [7], so that information concerning atmosphere, sea-ice and ocean will be simultaneously obtained. The goal of the lidar is to measure atmospheric profiles to get altitude and optical properties of aerosols and clouds. A network of such systems would also enable the study of aerosols transport across the Arctic. A first buoy equipped with a simple single wavelength backscattering lidar (i.e. no polarization) has been deployed in mid-April 2014, close to the North Pole. During about 8 months the buoy took measurements (four times a day, every six hours starting at 3 UTC) as it drifted toward the north of Svalbard, providing more than 750 atmospheric profiles as a whole. More recently two buoys were deployed during the first legs of the Norwegian New-ICE 2015 campaign (www.npolar.no), one with a polarizing backscattering lidar and the other with a non-polarizing system. Identification of the platforms deployed during these two campaigns is given in Table 1. The proximity of other instruments (e.g. radiometer) on the ice and on the boat will help for the ongoing analysis.

Table 1. Platforms deployed during the 2014 and 2015 campaigns

Plateform name	Lidar type	Year	Campaign	Location
IAOOS 2 (first fully equipped)	back[b]	2014	Barneo	north pole
IAOOS 4 & 7 [a]	back[b]	2015	N-ICE	Svalbard
IAOOS 6	polar[b]	2015	N-ICE	Svalbard

[a]IAOOS 4 and 7 use the same lidar
[b]"back" and "polar" respectively stand for "unpolarized" and "polarized" lidar

The all-new design of the first lidar systems developed within this project will be detailed in section 2. System performance are given and discussed with respect to simulations. Data corrections are presented in section 3 and first observations introduced in section 3 are more detailed in section 4.

2. Instrument description

A specific attention was paid to the design of the new autonomous lidar systems we wanted to deploy in arctic to optimize performance. A 2 year-autonomy was aimed at, and we chose to power the whole system with batteries, giving a limited available energy (a few watt.hours a day). A high efficiency laser diode based system (with central wavelength around 800 nm) was then chosen to be operated in emission sequences of 10 minutes, several times per day (up to 4 times 6 hours apart). The choice of low energy (a few microjoules per pulse) emission make this system to be identified as ceilometers. Standard ceilometers using 905 nm laser diodes are able to perform measurements of molecular scattering up to a range of 3-4 km during daytime depending on atmospheric transmission, which allow to use them for

Optics EXPRESS

boundary layer studies [8,9] and aerosols studies if a careful calibration is ensured [10]. Other designs use solid state laser Nd:Yag and offer similar range for measurements at 1064 nm [11]. Such instruments are now used in operational networks e.g. in the German meteorological network. The goal for aerosol lidar measurements is to meet high molecular backscattering sensitivity to get a good reference for calibration. A new design was adopted to perform our observations over the arctic ocean. To optimize the systems, the focus has been put on the detection performance in measuring molecular scattering at 4-5 km during daytime in arctic in clear air (without any cloud). One technological issue was thus to achieve a high overall efficiency along with a smaller sensitivity to water absorption, and a low temperature operation capability. A bi-axial system was chosen to minimize scattering at the emission. To optimize stability, the optical design was based on a bi-axial structure keeping a moderate field of view. The choice of an optical fiber based system has been led by thermal constraints, putting the sensitive parts (electronics, detector, laser diode) in the lower part of the buoy most frequently in contact of or at least near to the "warmer" arctic water (Fig. 1).

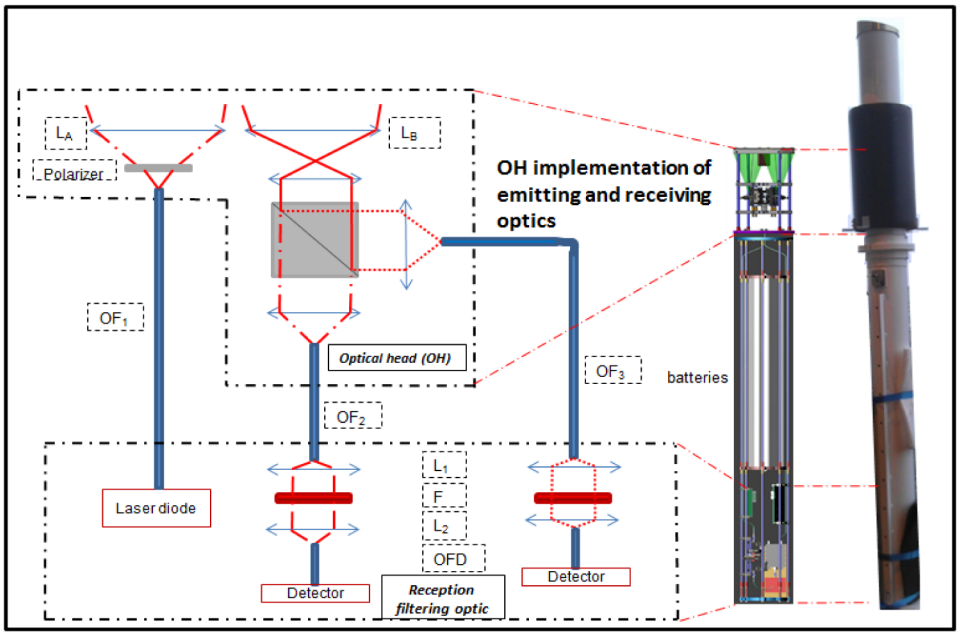

Fig. 1. Schematics and pictures of the polarized version of the IAOOS microlidar tube containing all the refractive optics and electronics. The sensitive parts are located in the bottom of the 3m long tube (right side) whose total weight when loaded is about 120kg. The optical connections to the lower part are made through the use of 2 meters optical fibers. The upper part of the tube is emerging 1 m above the buoy platform so that 1m of snow fall would not recover the window. Li stands for "Lens i", OFi for "Optical Fiber i" OFD for "Optical fiber to detector " and F for "Filter".

Due to the drift of the buoys with the ice pack on which they would be implemented, the laser systems were designed to be eye-safe (regarding the NF EN 60825-1 norm). Energy was therefore limited, and high frequency (5 to 10 kHz) operation along with a typical 10 minutes averaging sequence for each profile were adopted. Four sequences a day were aimed at to allow a sampling of cloud properties compatible with inputs/outputs of meteorological model analyses. The time duration of the sequence was chosen as a compromise between the optimization of the signal to noise ratio, the atmospheric variability, and the sampling need.

The optical head was developed at INSU by Division Technique, who also designed the control system and interface, as well as implementation. Realization of the lidar system was performed by the French company Cimel Electronique. Polarized emission for the second backscattering lidar system was based on the same design as for the standard system, but a

Optics EXPRESS

polarizing device and a polarization splitter were added at the emission and at the reception, respectively. A two-channel reception system was used to ensure dual polarization signal analysis. The detector is an Avalanche photodiode used in Geiger mode from Excelitas (formerly belonging to Perkin Elmer,). The photon counting signal is provided by a standard high-speed sampling and averaging electronic card from Cimel Electronique. The design is reported in Fig. 1. In the polarized design, the loss of about half of the energy emitted by the diode is compensated by increasing its operation current. In order to limit satellite communication costs each profile is only transmitted after averaging and summation, in progressively increasing altitude bins (Table 2). Background noise is determined from the upper channels. Accelerometers are implemented in the buoy, to provide with information concerning the tilt angles of the buoy as linked to potential ridge formation. All data are transferred to IPEV (http://iaoos.ipev.fr) using Iridium satellite link.

Table 2. Main characteristics of IAOOS 2 (and following plateforms) deployed during Barneo 2014

Parameters	Value
frequency / pulse width	~5 kHz / 200 ns
wavelength / bandwidth (FWHM)	~800 nm / < 0.6 nm
emitted energy / pulse	~2 µJ
diameter emission / reception lens	~70 mm
emission / reception full FOV	~650 µrad
detection filter bandwidth (FWHM)	~0.6 nm
overlap range (90%)	~300 m
detection sampling frequency (corresponding to a 15 m vertical resolution before averaging)	10Mhz
vertical resolution (after onboard averaging)	15 m [0-1 km] 30 m [1-3 km] 60 m [3-15 km] 120 m [15 –25 km]
background noise (average and standard deviation)	25 to 30 km

The main characteristics of the system are listed in Table 2. Since L_A and L_B, and OF_1 and OF_2 (or OF_3) (see Fig. 1), have the same properties, we may expect to have a similar divergence on both channels. A first calibration of the transmission of the system was performed in lab, using the emission diode. This transmission measurement involves the optics between the input/output fibers OF_2 (or OF_3) and OFD (see Fig. 1). To achieve this measurement a known optical power was injected at the input of OF_2 (or OF_3) transmitted through the different refractive optics then measured at the output of OFD. The ratio of the output of OFD and the input of OF_2 (OF_3) provides the transmission in the parallel and perpendicular polarization channels.

The electronics allows a sampling of the signal at a distance up to 30 km. The range between 25 and 30 km is used to determine the background noise (average value and standard deviation), as no strong backscattering is expected in this range.

First measurements after deployment allowed to check the range in clear air and overlap factor in real conditions. Range-corrected signals (RCSs) averaged over 10 minutes are reported in Fig. 2, for daytime (April 2014) and nighttime observations (November 2014). The molecular scattering adjusted on the RCS for nighttime (Fig. 2 (b)) is reported for daytime (Fig. 2 (a)), which fits upper level signal (at 3.2 to 4 km). In these figures we have also reported the range-corrected noise limit (standard deviation of the background noise multiplied by the range squared) allowing to identify the clear-air range of measurements as above 12 km for nighttime and around 3.5 km for daytime as the point of intersection with the average RCS (SNR = 1). As seen in Fig. 2, the overlap range identified as the range at which the signal is no longer rapidly increasing from the ground is located at about 300 m. The overlap function with range is determined from averaged clear air signals used for calibration.

Optics EXPRESS

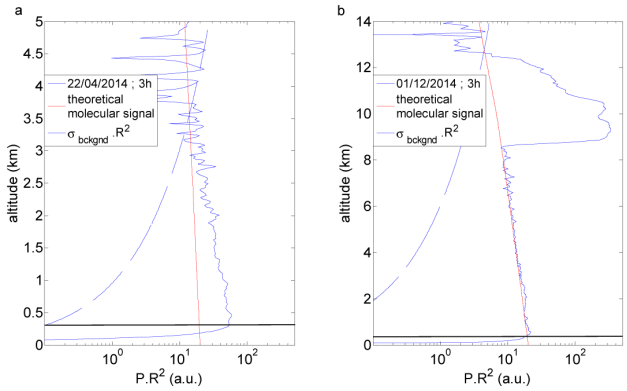

Fig. 2. Daytime (left) and nighttime (right) range corrected signals obtained after deployment of the buoy at Barneo in April 2014 (IAOOS 2). Solid black line is indicative of the overlap range.

Atmospheric calibration using molecular adjustment at night in the free troposphere allows to identify the presence of particles in the low or upper troposphere. One can see in Fig. 2 very unusually high cirrus clouds during nighttime and an extended layer of particles in the lower troposphere during daytime. As evidenced from previous field experiments, and presented later in this paper, larger backscattering in the lower troposphere are frequently occurring in spring in arctic [2]. Calibration was further checked with reference to molecular and dense water cloud scattering for various time periods, as will be discussed in next section.

3. Data correction and calibration

3.1 Data correction

Two main difficulties have been met in the analysis of the measured signals with the first deployments of this system, mostly linked to the use of an APD in photon counting mode. Saturation (or dead time limitation) is known to occur with this type of detector [12] and operating mode, in case of high backscattering signals (as due to clouds). This is highly dependent upon the efficiency of the electronics, associated to the APD, for quickly quenching the avalanche breakdown. Information is provided about the dead time for counts over 1 Mc/s by the manufacturer, but possible variation of the dead time with fluxes may be expected [13], which may cause uncertainties for high backscattering signals due to clouds and background. Measurements made in laboratory using a fixed target showed that the dead time value was stable at 20 +/–0.5 ns when varying the background level for a given energy emitted by the diode, and close to that provided by the manufacturer on the detector Performance Data sheet for counts below 1Mc/s (difference < 10%).

Another artifact that may be corrected is an undershoot effect due to oversaturation of the APD. After a dense cloud return, oversaturation was seen to occur, preventing the APD from counting correctly during several microseconds after the cloud. A strong decrease in signal (undershoot), biasing the cloud return signal is observed. A polynomial fit has been used to correct this undershoot, enabling the recovery of about a hundred meters of useful signal in the cloud.

Once these corrections are made, the average background light calculated in the upper channels (between 25 and 30 km) is subtracted to the signal in each bin. Overlap function O(r) and system constant C can then be determined from clear air signal analysis, writing the measured range-corrected signal (previously corrected from background noise) as

$$RCS(r) = C.O(r).(\beta_m + \beta_p)(r)T_m^{\,2}(r)T_p^2(r) \qquad (1)$$

T^2_m and T^2_p corresponds to the two-way transmission by molecules and particles, respectively. Several methods can be used to determine C, using the calibration on molecular

Optics EXPRESS

scattering, a lab calibration from detection of a known signal, or dense cloud return, and O(r) from atmospheric calibration from pure molecular return. We applied these methods related to atmospheric calibration, close to the lab and then in the field to perform additional correction due to modified overall transmission including the icing effect on the window.

3.2 Data calibration in clear air

An important difficulty in processing raw data came from spurious icing of the emission window, despite the built-in heating system. The icing problem is impacting the calibration of the IAOOS microlidar for a quantitative analysis of aerosol and cloud optical properties. However, as icing also increases the scattered signal by the emission window, measured just before the backscattered atmospheric signal, this information was used to determine a non-icing index (N-IcI), used to put aside too iced profiles, and possibly correct others. N-IcI is defined here from the ratio of the scattered signal on the iced window (IWS) to the clean window scattered signal (CWS) as N-IcI = CWS/IWS. It varies from 1 for a perfectly clear to 0 for a totally iced window.

Before being deployed, the optical transmission of IAOOS 2 has been measured in lab. A system constant of 7.8 +/– 0.8 10^4 was estimated.

By selecting backscattering profiles with identifiable molecular slope above the overlap range (between 0.5 and 8 km), over at least 1 km, and a IWS value close to the one measured in clear conditions (N-IcI > 0.98), we determined a reference system constant equal to C = 6.8 +/– 0.7 10^4. For this purpose, we selected two profiles at the end of the drift in nighttime clear arctic atmospheric conditions in November 2014. The constant was determined from attenuated scattering ratios (SR_{att}) defined as the ratio of the total attenuated backscattering coefficient ($\beta_m + \beta_p$) to the molecular backscattering coefficient (β_m) (see Eq. (2)) never exceeding 1 +/– 0.1 over a few hundreds of meters, after overlap factor correction and normalization to a pure molecular signal model (the molecular backscattering coefficient was derived here for simplification from standard subarctic atmospheric profiles [14]). SR_{att} can be a bit higher than 1 if there are some aerosols and lower than 1 if the transmission in the lower layers is not unitary.

$$SR_{att} = (1 + \frac{\beta_p}{\beta_m}).T^2 \tag{2}$$

This is in good agreement (12%, within error bars), with the lab determination. It confirms the good behavior of the system, considering the difference in operation temperature and transport of the system from Paris to Barneo.

The calibration correction factor (CCF) was defined as the ratio of the reference system constant in non-icing conditions (previously determined), to the system constant determined from the 10 profiles after normalization to the molecular scattering.

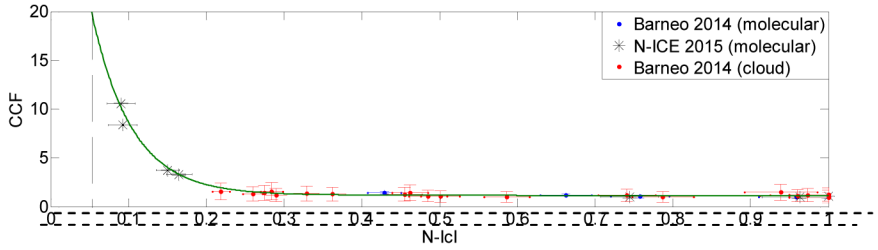

Fig. 3. Evolution of the calibration correction factor to be applied on the system constant as a function of the non-icing index using selected profiles with a molecular scattering zone near the surface (blue dots and black stars) and dense liquid water clouds (red dots) from 2014 campaign. The solid line shows the best exponential fit to the observations. The vertical dashed line shows the chosen limit of the applied correction (N-IcI > 0.05). Error bars are indicative of uncertainty in the correction.

Optics EXPRESS

Plotting the relative variation of the CCF as a function of the non-icing index N-IcI allowed to estimate corrections of the icing of the window for the two 2014-2015 campaigns as shown in Fig. 3. An exponential function was fitted to this curve. An estimate of the error is reported as vertical bars in the figure. It is estimated to 25% for N-IcI > 0.05.

We then used this function as a correction of the calibration for all the profiles depending on the window scattered signal and obtained the new system constants of the system for each measured profile. We limited the correction to an N-IcI value of 0.05, corresponding to a CCF value of 18 (Fig. 3). For profiles with N-IcI smaller than 0.05 the CCF is set equal to this value. We reported in Fig. 4(a) the variation of the system constant with time during the first period of the Barneo campaign (mid-April to July 2014). A slight decrease (about 12%, see dotted line in Fig. 4) may thus be seen for the most frequent top values (the ten upper profiles excepted corresponding to N-IcI above 0.92) between the mid of April (day 104) and the beginning of July (day 182). The observed decrease may be explained by an accumulation of ice crystals on the window as a function of time despite the built-in heating system, or by changes in the overlap and/or by low range scattering. Figure 4(b) presents the distribution function of the system constant. Most of the values are within 3 and 7.10^4, but about 35% are below the limit of correction.

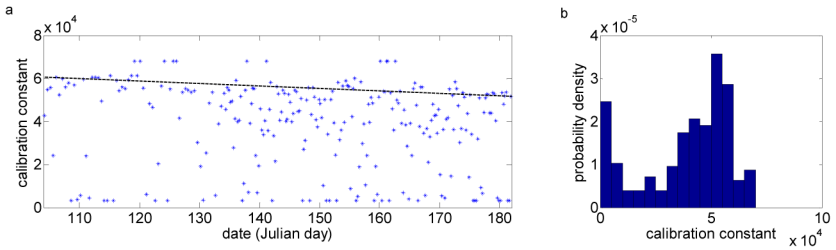

Fig. 4. a) System constants calculated for profiles from the first period of Barneo campaign, including icing correction. The line of points at the bottom represents measurements with a limited correction factor (N-IcI < 0.05). These points are removed in the analysis but kept in the probability density figure to show their distribution. b) Probability density function of system constants for the first period of the Barneo campaign. The peak on the left corresponds to the limitation of the correction factor. The dashed line corresponds to a fit of the maximum calibration values excepting the few clear window values.

This excluded about 250 profiles of the Barneo campaign from a more optimized correction, but measurements are flagged with the N-IcI so that they can be selected or not in the analysis. More than one hundred of points were not analyzed at the end of the drift (October and November, see next section) when the window was so iced that absolutely no signal was detected. Avoiding too-severe icing occurrence, profiles can at least be used for cloud occurrence analysis.

3.3 Data calibration and multiple scattering in cloudy conditions

High occurrence of low opaque water clouds in the Arctic during summer may be an advantage to monitor the calibration of the system. Based on O'Connor [15] work, this section is looking for deriving C. This however requires to estimate the multiple scattering coefficient in water clouds.

Let us consider the integrated range-corrected signal (IRCS) in the cloud derived from Eq. (1) rewritten as

$$IRCS = CT_a^2 \int_{cloud\ base}^{cloud\ top} (\beta_c + \beta_m).T_c^2 dz \qquad (3)$$

where T_a is the transmission from the surface to the cloud base, and β_c is the cloud backscattering coefficient. Cloud scattering is much larger than molecular scattering (especially true at the near infrared wavelength we are using), and one assumes it can be linked to cloud extinction as $\alpha_c = S_c.\beta_c$, where S_c is the lidar ratio for clouds. Using the

Optics EXPRESS

expression proposed by Platt for the integrated attenuated backscatter [16], the IRCS can be rewritten as

$$IRCS \approx \frac{CT_a^2}{2\eta S_c}(1-T_c^2) \tag{4}$$

where η is the average cloud multiple scattering factor. Looking for dense clouds implies a two-way transmission $T_c^2 = \exp -2\eta\tau_c$ close to zero, and assuming clear atmosphere ($T_a = T_m = 1$) below the cloud, the integrated cloud signal can be approximated to

$$IRCS \approx \frac{C}{2\eta S_c} \tag{5}$$

with a good accuracy.

For water clouds the value of S_c can be calculated from Mie theory to be close to 20 sr and this value is weakly varying (about 10%) with the cloud microphysical properties [17]. We first determined the η value from numerical simulations [18] as done in [15]. Using system parameters and a cloud droplet size of 6 µm for a cloud located between 4 and 4.3 km (with scattering coefficient of 0.0168 m^{-1}), one can estimate a value of η = 0.92+/–0.03 (the uncertainty stands for the variation of η in the cloud with altitude). This value is close to those obtained for similar ground based systems [15].

On the other hand, the system constant was determined in Paris for IAOOS 6 using the standard molecular normalization method, looking to the parallel polarization signal. We obtained with this method a system constant C ~6.7 10^4 +/– 0.9, very close to that obtained with IAOOS 2 (atmospheric depolarization in dust-free atmosphere remains small < 5%). We then considered measurements in dense stratocumulus clouds over Paris and, following Eq. (5), using S_c = 20 sr and the previous = value of C found in clear air, we derived η = 0.80 +/–0.05 from the signal integration in the cloud. This value is smaller than the estimation from the model, for which only droplets with diameter of 50 µm would allow to derive such a low theoretical multiple scattering factor. This will require further investigations.

4. Results

4.1 Non-polarized system

The first fully equipped IAOOS buoy (IAOOS 2) was placed in the iced arctic ocean at the North Pole (Barneo camp) on April 15, 2014. The measurements then taken during the drift showed a very good behavior of the whole system, with no unexpected power consumption in arctic cold conditions, and very few profiles lost because of satellite communications. The 2014 drift provided about 750 profiles of total backscattering profiles in the area 80-88°N and 10-25°E. Attenuated scattering ratios SR_{att} obtained after data correction, calibration and normalization to molecular scattering are reported in Fig. 5. The inclination of the buoy is also reported on the same figure. It shows that the buoy was close to zenith in spring (tilt of about 1°), and experienced a strong tilt due to a compression ridge at day 183 (early July), and then recovered at the end of August. Another tilt occurred in early October as floes were telescoping. In the beginning of the first period, near days 110 to 130 (mid-April to mid-May), numerous measurements were showing low attenuated scattering ratios (no low cloud) and such low values (SR_{att} varying from 1 to 3, which corresponds to less than 20% of the overall cases) may be attributed to the presence of aerosols and/or haze which increased the signal, sometimes without significantly modifying the expected molecular slope.

Optics EXPRESS

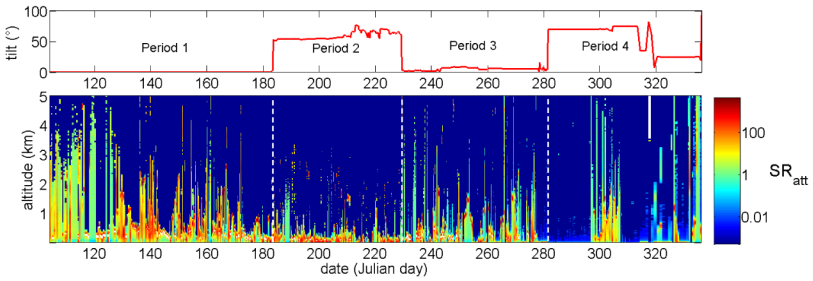

Fig. 5. Temporal and vertical variation of the attenuated scattering ratio derived over the whole drifting period of the 2014 campaign (IAOOS 2) obtained with calibration correction based on the measured window icing index. Dashed lines delimit the different periods depending on the tilt of the buoy, as reported in the upper part of the figure. The different tilts are due to the motion of ice and more particularly compression and deformation of ice floes where they are weaker. Trustful values are obtained over the whole data set, except where icing is too strong (for example between day 278 and 299).

Detection of cloud bases and tops was made over vertical profiles of the attenuated scattering ratio, regardless of the magnitude of the non-icing index. This first analysis showed a large occurrence of very low clouds with a cloud base frequently below 1km of altitude (and even 500m). The frequency of such very low clouds is as high as 60%. It mostly appears to be supercooled water clouds, as identified from their strong scattering ratio and large extinction extinction leading to narrow signal peaks and temperatures between −10 and −30 °C estimated from meteorological analyses. The probability densities of occurrence of the maximum SR_{att} values, and corresponding altitudes are reported in Fig. 6 for the first period of the Barneo campaign. Adjusted gamma and exponential distributions are given for the peak SR_{att} and peak altitude, respectively. The average values of the altitude and attenuated lidar scattering ratio are about 0.8 km and 900 respectively, whereas the median values are about 0.5 km and 600, respectively.

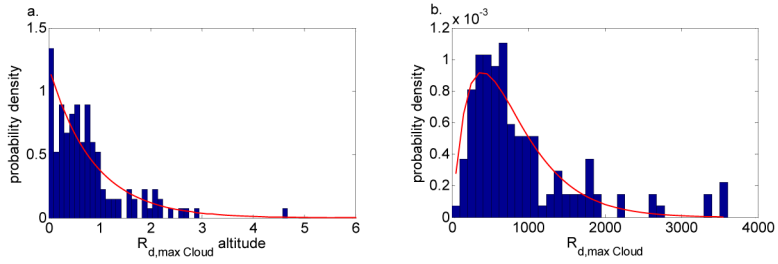

Fig. 6. a. Probablity density functions (Pdf) of altitudes of the maximum values of attenuated scattering ratio. b. Pdf of the maximum values of the attenuated scattering ratio of the detected clouds. This was obtained for the period 1 of the 2014 campaign (IAOOS 2).

These distributions are in good agreement with measurements made during SHEBA [2] which showed monthly averaged cloud base height around 1km and lowest cloud base height below 500 m. The data obtained during these three months of 2014 in the western arctic basin however show smaller values and tend to show more low level clouds than during SHEBA, organized more than 15 years ago over the eastern part of the Arctic Ocean.

4.2 Polarized system

The N-ICE2015 campaign was the opportunity to test the new polarization set up of the microlidar, and to obtain more information on the system behavior during wintertime. An example of profiles obtained at 83°N in February 2015 is shown in Fig. 7. IAOOS 6 was deployed in the ice, a few degrees from zenith pointing according to inclination sensors in the lidar tube. The total attenuated backscattering coefficient profiles in Fig. 7 were obtained by

Optics EXPRESS

assuming a similar system constant for both reception channels. The value used for the system constant has been deduced from the quasi-molecular signal below the cloud in the parallel channel and assuming a 90% atmospheric two-way transmission. This value is based on measurements from the integrated signal and the AERONET network (http://aeronet.gsfc.nasa.gov) made at the observation sites of PEARL (Polar Environment Atmospheric Research Laboratory) in Canada and Hornsund (Svalbard).

For the parallel channel (continuous blue curve in Fig. 7) the slope below the clouds corresponds to a probably low aerosol contribution superimposed on molecular scattering (1.5 - 4.5 km).

Calibration of the depolarization was performed in Paris with the method detailed in [19] and [20]. An alignment uncertainty of about 2° between transmitter and receiver polarization axes was identified, leading to a potential crosstalk between channels and thus a bias in depolarization [20,21]. A volume linear depolarization ratio (hereafter called "depolarization ratio") higher than molecular theoretical value (0.36% with the single selection of the Cabannes line [22]), is reported in Fig. 7. The measured signal about three times higher than theory for pure molecular backscattering, as observed here, may be due to the particles seen below the cloud in the parallel channel, but also to the identified cross-talk between channel, due to a biased calibration. The existence of a small unpolarized component in the emitted laser beam is unlikely thanks to the use of a polarizer at the emission (see Fig. 1) with high contrast (about 1:100000). To reduce uncertainty and bias in the next systems, an improved calibration control is of main importance for future systems needs to be deployed. The present calibration error still allows to separate spherical aerosols and oriented ice crystals having depolarization ratios smaller than 10% (as seen below 5 km), from randomly oriented ice crystals with depolarization larger than 30%. Water clouds are showing progressively increasing depolarization as the beam propagates through the cloud, and its value is depending on the cloud optical depth [23].

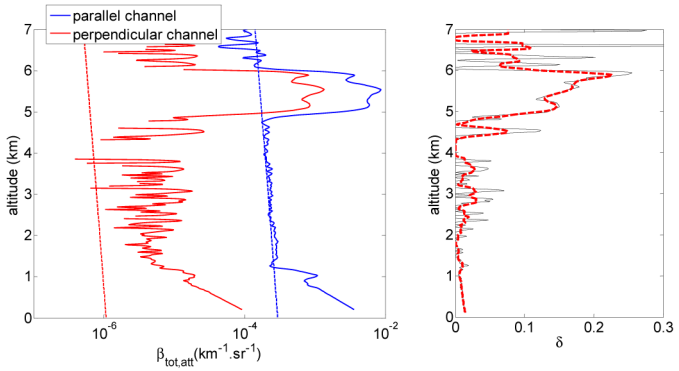

Fig. 7. left: total attenuated backscatter coefficient measured in both co- and cross-polarizations during the N-ICE2015 campaign (IAOOS 6), assuming a similar system constant, with theoretical normalized molecular signal as dashed lines (assuming a 0.36% depolarization for the red), and right: depolarization ratio obtained with calibration by polarization rotation method, and with convolution over 200m for the red dashed curve. See text for discussion of uncertainties and biases.

The N-ICE2015 campaign did not allow to unambiguously identify particles, giving depolarization ratio as low as 15-22% . These values were observed as the cloud base was given at a temperature about –48°C according to radiosonde launched from the near-by station of Ny-Alesund. At this temperature, liquid water cannot be found, but a few oriented crystals may still be present at cloud base. The measured depolarization ratios are nevertheless consistent with finding from space observations at this latitude [24].

Optics EXPRESS

5. Conclusions

The development of first autonomous microlidar systems has been achieved in the frame of the IAOOS project. Their first deployment on drifting buoys in the arctic has been fairly successful. A first drift performed in 2014 with a non-polarizing system lasted during almost 8 months. Very few measurements were lost because of satellite communication. The system operated as planned in the range of external temperatures from −40 to + 5°C. Two to four lidar atmospheric profiles a day were transmitted during this first drift. Moderate icing (non-icing index larger than 0.15) periods were observed from spring to autumn and corrections in signal transmission could be made in about 54% of cases, using the signal backscattered by the window at the emission time. Another deployment performed in the winter and spring period was performed within the N-ICE2015 campaign to test a dual polarization system. Severe icing periods were observed in winter. Although solutions could be found as explained in our analyzis to face moderate icing conditions, severe icing is an important limitation to get a proper and stable calibration of the system. Solutions for avoiding icing of the window, as experienced mostly during the end of autumn, and winter period have to be improved for forthcoming deployed systems. Outside severe icing periods, valuable statistical analyzes could be started on the data obtained in Central Arctic. Results show the high occurrence of very low level arctic clouds, with an average altitude lower than 800 m in the period going from end of spring to end of autumn at latitudes higher than 82°N. Polarization information is also of importance to better describe cloud properties and identify the occurrence of spherical aerosol particles. A more detailed analysis of the data acquired during the two campaigns introduced here is underway, including retrieval of aerosols backscatter coefficients using lidar signal inversion methods. New deployments are planned in the coming years to further test improvements aiming at regular measurements of aerosols and clouds during the longest period as possible in the Arctic.

Funding

Agence Nationale de la Recherche (ANR-10-EQPX-32-01); Seventh Framework Program (ICE-ARC 603887).

Acknowledgment

We are thankful to the DT/INSU/CNRS for the mechanical and system design as well as tests of the microlidar and buoy set up in the arctic. We also would like also to thank the Association Nationale de la Recherche et de la Technologie and CIMEL Electronique for supporting the PhD work of V. Mariage.